Kinetic Study of IO Radical with RO_2 (R = CH_3, C_2H_5, and CF_3) Using Cavity Ring-Down Spectroscopy

Shinichi Enami, Takashi Yamanaka, Satoshi Hashimoto, and Masahiro Kawasaki*

Department of Molecular Engineering, Kyoto University, Kyoto 615-8510, Japan

Yukio Nakano and Takashi Ishiwata

Faculty of Information Sciences, Hiroshima City University, Hiroshima 731-3194, Japan

Received: March 29, 2006; In Final Form: May 18, 2006

The reactions of iodine monoxide radical, IO, with alkyl peroxide radicals, RO_2 (R = CH_3, C_2H_5, and CF_3), have been studied using cavity ring-down spectroscopy. The rate constant of the reaction of IO with CH_3O_2 was determined to be $(7.0 \pm 3.0) \times 10^{-11}$ cm^3 molecule^{-1} s^{-1} at 298 K and 100 Torr of N_2 diluent. The quoted uncertainty is two standard deviations. No significant pressure dependence of the rate constant was observed at 30−130 Torr total pressure of N_2 diluent. The temperature dependence of the rate constants was also studied at 213−298 K. The upper limit of the branching ratio of OIO radical formation from IO + CH_3O_2 was estimated to be <0.1. The reaction rate constants of IO + $C_2H_5O_2$ and IO + CF_3O_2 were determined to be $(14 \pm 6) \times 10^{-11}$ and $(6.3 \pm 2.7) \times 10^{-11}$ cm^3 molecule^{-1} s^{-1} at 298 K, 100 Torr of N_2 diluent, respectively. The upper limit of the reaction rate constant of IO with CH_3I was $<4 \times 10^{-14}$ cm^3 molecule^{-1} s^{-1}.

1. Introduction

The atmospheric chemistry of IO_x radicals has attracted attention for their potential effect on the catalytic destruction of ozone[1−4] and on particulate formation[5−9] in the marine boundary layer (MBL). The IO radical affects the concentration of ozone in the troposphere, because it is involved in the ozone depleting cycle through reactions with HO_2, NO_2, and IO itself. Model calculations show that 15−40%[10] and up to 50%[11,12] of the troposphere ozone loss could be explained by such iodine chemistry, although there are still many unknown parameters, e.g., the rate constants for radical reactions. Peroxy radicals, RO_2 radicals, could be candidates for consumers of IO, since RO_2 radicals have been measured in the MBL at mixing ratios of 40−80 pptv.[13] Recently, Bale et al. reported the rate constant of IO with methyl peroxy radical, the most abundant peroxy radical, at room temperature under 2.5 Torr He diluent using a discharge-flow tube.[4]

$$CH_3O_2 + IO \rightarrow CH_3O + OIO \quad \Delta H^4 = -30.7 \text{ kJ mol}^{-1} \tag{1a}$$

$$\rightarrow CH_3O + IOO \quad \Delta H^4 = -11.1 \text{ kJ mol}^{-1} \tag{1b}$$

$$\rightarrow CH_2O_2 + HOI \quad \Delta H^4 = -6.5 \text{ kJ mol}^{-1} \tag{1c}$$

$$\rightarrow CH_3OI + O_2 \quad \Delta H^4 = -171.8 \text{ kJ mol}^{-1} \tag{1d}$$

In this paper, we have measured the rate constants of IO + CH_3O_2 at 213−298 K and 30−130 Torr total pressure of N_2 diluent using cavity ring-down spectroscopy (CRDS).[14−16] The reactions of IO with $C_2H_5O_2$ and CF_3O_2 have also been studied.

$$C_2H_5O_2 + IO \rightarrow \text{products} \tag{2}$$

$$CF_3O_2 + IO \rightarrow \text{products} \tag{3}$$

The reaction of IO with CF_3O_2 was recently studied by Bale et al.,[4] which is important for laboratory kinetic study of IO radicals such as IO + CH_3SCH_3.[17]

2. Experimental Section

The CRDS apparatus used in the present study has been described elsewhere.[18] The system employs a photolysis laser (Spectra Physics, GCR-250) and a probe laser (Spectra Physics, MOPO-SL, spectral resolution 0.2 cm^{-1}). After the photolysis laser pulse beam traverses a glass tube reactor, the probe laser pulse beam is injected nearly collinear to the axis of the photolysis laser through one of two high-reflectivity mirrors. The cavity ring-down mirrors (II-VI Co. or Research Electro-optics, 7.8-mm diameter and 1-m curvature) have a specified maximum reflectivity of 0.9997 and are mounted 1.04 m apart. Light leaking from the end mirror is detected by a photomultiplier tube (Hamamatsu Photonics, R212UH) through suitable band-pass filters (Edmund Optics). The length of the reaction region is 0.40 m. Temporal decay of the light intensity is recorded using a digital oscilloscope (Tektronix, TDL-714L, 8-bit resolution) and transferred to a personal computer. In the presence of an absorbing species, the light intensity within the cavity is given by expression 4

$$I(t) = I_0 \exp(-t/\tau) = I_0 \exp(-t/\tau_0 - \sigma n c L_R t/L_C) \tag{4}$$

where I_0 and $I(t)$ are the light intensities at time 0 and t, τ is the cavity ring-down time with photolysis beam, τ_0 is the cavity

* To whom correspondence should be addressed. Fax number: + 81−75−383−2573. E-mail address: kawasaki@moleng.kyoto-u.ac.jp.

10.1021/jp0619336 CCC: $33.50
Published on Web 07/20/2006

ring-down time without photolysis laser light (typically 5 μs), L_R is the length of the reaction region (0.40 ± 0.01 m), L_C is the cavity length (1.04 m), c is the velocity of light, and n and σ are the concentration and the absorption cross section of absorbing species, respectively. A value of $\sigma_{IO} = 5.9 \times 10^{-17}$ cm^2 molecule^{-1} at 435.63 nm, which was determined by the same spectral resolution in the present study, is used to calculate the absolute concentration of IO.[17] We assume that the error in the estimation of the absolute concentration of IO is within 20%, considering the uncertainties in extrapolation for the $[IO]_0$ concentration as well as those of pressure, mass flow rates, reaction path length, and fluctuation of photolysis laser power. By varying the delay between the photolysis and probe laser pulses, the concentration of IO is monitored as a function of delay time. Each ring-down trace is digitized with a time resolution of 20 ns. The digitized traces are transferred to a computer and averaged over 16 or 32 runs to calculate the ring-down rate, τ^{-1}. The validity of using of cavity ring-down spectroscopy for kinetic studies derives from the fact that the lifetimes of the products generated by photolysis are much longer than the associated cavity ring-down times.[19]

Ozone is produced by irradiating an oxygen gas flow with the 184.9-nm output of a low-pressure Hg lamp (Hamamatsu Photonics, L937), and its concentrations are measured upstream of the reaction tube by monitoring the absorption at 253.7 nm ($\sigma = 1.15 \times 10^{-17}$ cm^2 molecule^{-1})[20] using a separate low-pressure Hg lamp as a light source. Typical concentrations of O_3 and O_2 are 1.6×10^{13} and 3.2×10^{17} molecule cm^{-3}, respectively. The 266-nm output of the Nd^{3+}:YAG laser is used to dissociate O_3 to give $O(^3P) + O_2$. Although appreciable amounts of $O(^1D)$ are produced, they are electronically quenched to $O(^3P)$ within 0.2 μs in our experimental conditions.[20] Hence, no reactions of $O(^1D)$ with any other species occurred.

The reaction cell, consisting of a Pyrex glass tube (21-mm i.d.), is evacuated by the combination of an oil rotary pump, a mechanical booster pump and a liquid N_2 trap. The temperature of the gas flow region is controlled over the range 213−298 K by circulation of ethanol with a cooling circulator (Thomas, TRL 70 SLP). The difference between the temperatures of the sample gas at the entrance and exit of the flow region is measured to be <1 K. The pressure in the cell is monitored by an absolute pressure gauge (Baratron, 622A). A slow flow of nitrogen diluent gas is introduced at the ends of the ring-down cavity, close to the mirrors, to minimize deterioration caused by exposure to the reactants and the products in the cell. The total flow rate is adjusted (typically 2000 sccm) so that the gas in the cell is replaced completely within the 0.5-s time intervals between photolysis laser pulses.

Sample gases for CH_3I, C_2H_5I, and CF_3I are prepared in a glass gas bulb with N_2 diluent. Then, the mixture gas is injected into a glass reaction cell by mass flow controllers (STEC, SEC-E40). Concentrations of these compounds in the reaction cell are calculated by the flow rates. All reagents are obtained from commercial sources. CH_3I (>99.5%) is obtained from Sigma Aldrich, and C_2H_5I (>99%) is obtained from Wako Pure Chemicals, which are subjected to freeze−pump−thaw cycling before use. CF_3I (>99%, Apollo Scientific), N_2 (>99.999%, Teisan Co.), and O_2 (>99.995%, Teisan Co.) are used without further purification.

3. Results

Reaction of IO with CH_3O_2. IO is formed by the reaction of $O(^3P)$ with CH_3I.[21]

$$O(^3P) + CH_3I \rightarrow IO + CH_3 \quad (5a)$$

$$\rightarrow CH_2I + OH \quad (5b)$$

Following reaction 5b, CH_2I is consumed by the reaction of O_2 to generate another IO.[22]

$$CH_2I + O_2 \rightarrow IO + HCHO \quad (6)$$

Using the branching ratios for reactions 5a and 5b reported by Gilles et al.,[21] the total yield of IO from the reaction of CH_3I with $O(^3P)$ in the presence of O_2 was estimated to be (0.6 ± 0.2) at 298 K.[22]

Another possible source of IO is the reaction of I atoms with O_3 from the photodissociation of CH_3I at 266 nm. However, IO generation from $I + O_3$ was minor in our experimental conditions because of the low O_3 concentration (below 2.5×10^{13} molecule cm^{-3}) and relatively small rate constant. We estimated the reaction rate of IO formation from $I + O_3$ to be <30 s^{-1}.

CH_3O_2 radicals were generated by reactions 7 and 8 under an excess amount of O_2 (>10^{17} molecule cm^{-3}) within a few microseconds in our experimental conditions.

$$CH_3I + h\nu_{266\,nm} \rightarrow CH_3 + I \quad (7)$$

$$CH_3 + O_2 + M \rightarrow CH_3O_2 + M \quad (8)$$

Radical concentration of IO was monitored at 435.63 nm, which is the band head of the $A^2\Pi_{3/2} \leftarrow X^2\Pi_{3/2}$ (3, 0) transition.[23] The inset of Figure 1 shows the cavity ring-down spectrum of IO. The signal baseline was taken at 435.00 nm, a region in which there is no IO absorption. The IO concentration profile was measured between 0.1 and 8.0 ms after the photolysis laser pulse. Figure 1 shows a typical decay profile of the IO concentration with CH_3I of 1.2×10^{15}, O_2 of 3.2×10^{17}, and O_3 of 1.6×10^{13} molecule cm^{-3} at 298 K in 100 Torr total pressure of N_2 diluent. A simple pseudo-first-order analysis was not applicable to the present kinetic analysis, because CH_3O_2 decreases by reactions and diffusion loss. Therefore, numerical models were compiled using the chemical equations listed in Table 1 in order to derive the rate constants of IO + CH_3O_2.

In our experimental conditions, IO was consumed mainly by the reaction with CH_3O_2 via reaction 1, since 10−100-fold excess amounts of CH_3O_2 over IO were used. The diffusion loss rate from the detection region was determined to be (200 ± 50) s^{-1} from the best fits of simulation for several decays and was used for all other simulations. The self-reaction of IO also contributes to the decay of IO,[24] but the contribution should be minor because of the relatively low concentration of IO. The initial concentrations of CH_3 and I, $[CH_3]_0$ and $[I]_0$, were derived by the following equations;

$$[CH_3]_0 = [I]_0 = \frac{\sigma_{CH_3I}[CH_3I][O]_0}{\sigma_{O_3}[O_3]} \quad (9)$$

$$[IO]_0 = \alpha[O]_0 \quad (10)$$

The absorption cross sections, $\sigma_{CH_3I} = 1.0 \times 10^{-18}$ cm^2 molecule^{-1} and $\sigma_{O_3} = 9.4 \times 10^{-18}$ cm^2 molecule^{-1}, were quoted from the NASA recommended values.[20] $\alpha = (0.6 \pm 0.2)$ is quoted from the reported total yield of IO for reactions 5a and 5b at 298 K.[21] $[IO]_0$ was obtained by extrapolation of the experimentally observed decay of the concentration of IO to t_0. To confirm the procedure, we compared the extrapolated values

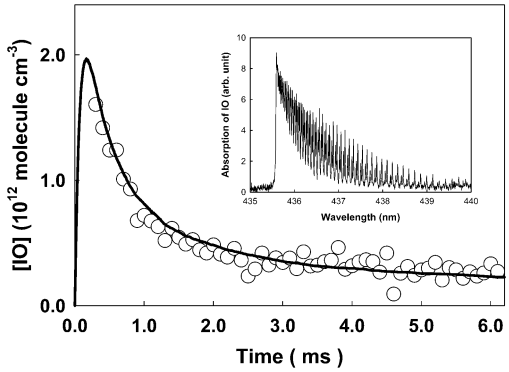

Figure 1. A typical decay time profile of IO in the presence of CH_3O_2 at 298 K and 100 Torr total pressure of N_2 diluent. $[CH_3I] = 1.2 \times 10^{15}$, $[O_3] = 1.6 \times 10^{13}$, $[CH_3]_0 = 2.3 \times 10^{13}$ molecule cm^{-3}. The thick curve is the result of simulations (see text for details). The inset shows the cavity ring-down spectrum of IO measured from photodissociation of the mixture of $O_3/O_2/CF_3I$ at 266 nm.

TABLE 1: Reactions Used in Kinetic Simulation for IO + CH_3O_2 at 298 K and 100 Torr Total Pressure of N_2 Diluent

reaction	rate constant (cm^6 molecule^{-2} s^{-1} or cm^3 molecule^{-1} s^{-1} or s^{-1})	ref
$CH_3I + O(^3P) \rightarrow IO + CH_3$	7.8×10^{-12}	21
$\rightarrow OH + CH_2I$	2.4×10^{-12}	21
$CH_2I + O_2 \rightarrow IO + HCHO$	4.0×10^{-13}	22
$CH_3I + OH \rightarrow CH_2I + H_2O$	7.4×10^{-14}	20
$I + O_3 \rightarrow IO + O_2$	1.2×10^{-12}	20
$IO + CH_3O_2 \rightarrow$ products	best-fit parameter	this work
$2\,IO \rightarrow OIO + I$	3.3×10^{-11}	26
$\rightarrow 2I + O_2$	8.2×10^{-12}	26
$\rightarrow$ others	4.1×10^{-11}	26
$I + IO \rightarrow I_2O$	2.2×10^{-11}	*a*
$I_2O + I \rightarrow I_2 + IO$	2.1×10^{-10}	26
$IO + O \rightarrow I + O_2$	1.4×10^{-10}	41
$CH_3 + O_2 + M \rightarrow CH_3O_2 + M$	4.4×10^{-31}	20
$2CH_3O_2 \rightarrow 2CH_3O + O_2$	1.3×10^{-13}	42
$\rightarrow$ others	2.1×10^{-13}	42
$CH_3 + CH_3O_2 \rightarrow 2CH_3O$	2.0×10^{-11}	4
$CH_3O + O_2 \rightarrow HO_2 + HCHO$	1.9×10^{-15}	20
$CH_3O_2 + CH_3O \rightarrow$ products	1.0×10^{-12}	20
$HO_2 + IO \rightarrow HOI + O_2$	8.4×10^{-11}	20
$HO_2 + I \rightarrow HI + O_2$	3.8×10^{-13}	20
$IO + CH_3O \rightarrow$ products	4.0×10^{-11}	43
$I + CH_3O \rightarrow$ products	8.5×10^{-11}	43
$I + CH_3O_2 \rightarrow$ products	3.7×10^{-11}	*b*
$I + CH_3 \rightarrow CH_3I$	1.0×10^{-11}	44
$I + I + M \rightarrow I_2 + M$	1.0×10^{-32}	45
$O + O_2 + M \rightarrow O_3 + M$	5.9×10^{-34}	20
diffusion rate	200	this work

[a] Pressure correction was performed. See text for details. [b] Same value for the reaction of I with CF_3O_2 was assumed. See text for details.

with those obtained by simulation. The simulation results reproduce the obtained decay time profiles of IO. The discrepancy between two estimated $[IO]_0$ was within 10%. We include this uncertainty to the error to final k. Concentrations of CH_3O_2 were experimentally changed by using different concentrations of CH_3I and O_3, and by changing the dissociation laser intensity.

The effects of the secondary reactions were carefully checked. For example, IO-catalyzed iodine atom recombination could affect the analysis by undergoing the following reactions.[25,26]

$$IO + I + M \rightarrow I_2O + M \quad (11)$$

$$I_2O + I \rightarrow I_2 + IO \quad (12)$$

Bloss et al. reported the rate constants of reactions 11 and 12

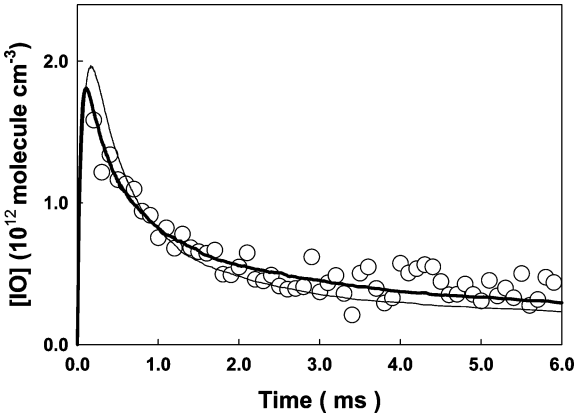

Figure 2. A typical decay time profile of IO in the presence of CH_3O_2 at 213 K and 100 Torr total pressure of N_2 diluent. $[CH_3I] = 2.8 \times 10^{15}$, $[O_3] = 2.2 \times 10^{13}$, $[CH_3]_0 = 3.0 \times 10^{13}$ molecule cm^{-3}. The thick curve is the result of simulations. The thin curve is the result of simulations at 298 K for comparison.

to be 1.7×10^{-10} and 2.1×10^{-10} cm^3 molecule^{-1} s^{-1} at 295 K and 760 Torr, respectively.[26] As for reaction 11, we adjusted the rate constant for the pressure difference of N_2, that is, $(1.7 \times 10^{-10}) \times (100\ \text{Torr}/760\ \text{Torr}) = 2.2 \times 10^{-11}$ cm^3 molecule^{-1} s^{-1} for our simulations assuming that reaction 11 is in pure third order up to the pressure used. However, we found that the calculated decays of IO were not sensitive to reactions 11 and 12 but sensitive mostly to reaction 1. Even if we used the value 1.7×10^{-10} cm^3 molecule^{-1} s^{-1} for the rate constant of reaction 11, no change was observed in the calculated IO decay. The reaction of CH_3O_2 with I atom may also occur in our system, although no formation of IO from $CH_3O_2 + I$ was previously observed.[22] Because the rate constant of $CH_3O_2 + I$ has not been reported, we used the value 3.7×10^{-11} cm^3 molecule^{-1} s^{-1}, which was the reported rate constant for $CF_3O_2 + I$.[27] For the reaction of IO with CH_3I, the upper-limit value of the rate constant of IO with CH_3I was derived to be very small, 4×10^{-14} cm^3 molecule^{-1} s^{-1}, by changing the concentrations of CH_3I and the laser intensity. Hence, the reaction of IO with CH_3I did not affect the kinetics of IO + CH_3O_2.

We found experimentally that k_1 had no dependence on the concentration of CH_3I in the range $(1.0-6.0) \times 10^{15}$ molecule cm^{-3}, nor on the photodissociation laser intensity in the range 35−58 mJ pulse^{-1}. These results indicate that k_1 is independent of the initial concentrations of CH_3 radicals and I atoms. With best-fit procedures, k_1 was obtained to be $(7.0 \pm 1.4) \times 10^{-11}$ cm^3 molecule^{-1} s^{-1} at 100 Torr total pressure of N_2 diluent as shown in Figure 1. We recommend the value $(7.0 \pm 3.0) \times 10^{-11}$ cm^3 molecule^{-1} s^{-1} considering the all uncertainties of σ_{IO}, α, estimation of $[IO]_0$, measurements in pressure, mass flow rates, and reaction path length, and simulation fittings. It is noted that no significant pressure dependence of k_1 was observed within 30% of error bar range for the total pressures of 30, 70, 100, and 130 Torr. Therefore, the present value of k_1 could be applied to atmospheric modeling.

We also conducted the experiments at lower temperatures. Figure 2 shows a typical time profile of IO at 213 K. When analysis of the temperature dependence of k_1 was performed, temperature-dependent reactions in Table 1, e.g., $CH_3I + O(^3P)$, were taken into account. At lower temperatures, $O(^3P)$ is also consumed by the reaction with O_2. Therefore, the initial concentrations of CH_3 and I were estimated by the simulations without using eqs 9 and 10. The rate constant, k_1 for 213−298 K at 100 Torr, shows a weak positive temperature dependence (see Table 2 and Figure 3). Arrhenius analysis resulted in the

TABLE 2: Temperature Dependence of the Rate Constant for IO + CH_3O_2

temperature (K)	rate constant (10^{-11} cm^3 molecule^{-1}s^{-1})
213	5.4 ± 1.1
233	5.8 ± 1.2
253	6.0 ± 1.2
273	6.2 ± 1.2
298	7.0 ± 1.4

activation energy of 1.4 ± 0.6 kJ mol^{-1} and a preexponential factor of 1.3×10^{-10} cm^3 molecule^{-1} s^{-1}.

Product Branching Ratios. Formation of OIO radical from reaction 1a was investigated by trying to detect the CRDS signal of OIO at 549.1 nm. OIO formation from 266/355-nm irradiation of $CH_2I_2/O_2/N_2$ mixtures was successfully confirmed with our CRDS method, as shown in the inset of Figure 4. OIO was produced from reaction 6 followed by the self-reaction of IO. We also observed the same signal intensity of OIO from 355-nm irradiation in the presence of O_3 ($[O_3] = 1.6 \times 10^{13}$ molecule cm^{-3}), which means that the reaction of OIO with O_3 was not important in our experimental conditions. Then, we attempted to detect OIO under the following condition: $[CH_3I] = (1.0-2.4) \times 10^{15}$, $[O_3] = 1.6 \times 10^{13}$, and $[O_2] = 3.2 \times 10^{17}$ molecule cm^{-3} at 298 K and 100 Torr total pressure of N_2 diluent. The dissociation laser intensity at 266 nm was 53 mJ pulse^{-1}. However, we could not find any evidence of OIO signals from reaction 1a. Expected time profiles of OIO from the reaction of IO with CH_3O_2 with the branching ratios of 0 and 0.1 were shown in Figure 4. From our detection limit of OIO, which

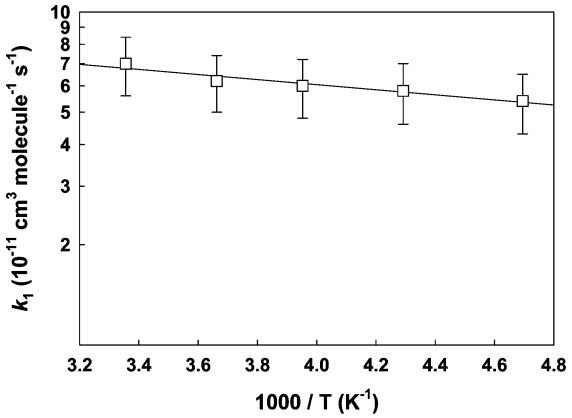

Figure 3. Temperature dependence of the rate constant of IO + CH_3O_2.

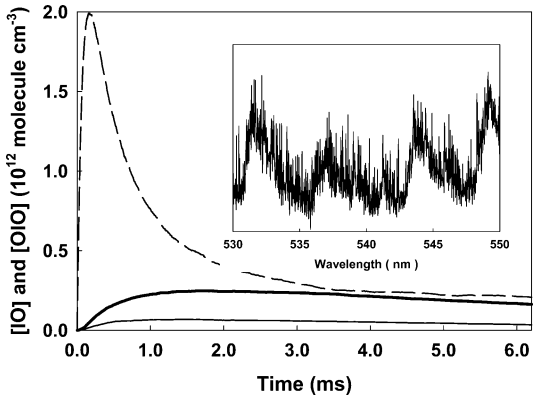

Figure 4. Simulated time profiles of IO (broken curve) and OIO with $Y_{OIO} = 0.1$ (thick curve) and $Y_{OIO} = 0$ (thin curve). $[CH_3I] = 1.2 \times 10^{15}$, $[O_3] = 1.6 \times 10^{13}$, $[CH_3]_0 = 2.3 \times 10^{13}$ molecule cm^{-3}. The inset shows a reference spectrum of OIO (including I_2) from the irradiation of 266 nm of a mixture of $CH_2I_2/O_2/N_2$.

TABLE 3: Reactions Used in Kinetic Simulation for IO + $C_2H_5O_2$ at 298 K, 100 Torr Total Pressure of N_2 Diluent[a]

reaction	rate constant (cm^6 molecule^{-2} s^{-1} or cm^3 molecule^{-1} s^{-1} or s^{-1})	ref
$C_2H_5I + O(^3P) \rightarrow IO + C_2H_5$	7.0×10^{-12}	29
$\rightarrow HOI + C_2H_4$	2.8×10^{-11}	29
$IO + C_2H_5O_2 \rightarrow$ products	best-fit parameter	this work
$C_2H_5 + O_2 + M \rightarrow C_2H_5O_2 + M$	1.5×10^{-28}	20
$2C_2H_5O_2 \rightarrow 2C_2H_5O + O_2$	4.0×10^{-14}	42
$\rightarrow$ others	2.4×10^{-14}	42
$C_2H_5 + C_2H_5O_2 \rightarrow 2C_2H_5O$	2.0×10^{-11}	*b*
$C_2H_5O_2 + C_2H_5O \rightarrow$ products	1.0×10^{-12}	*b*
$C_2H_5O + O_2 \rightarrow HO_2 + CH_3CHO$	1.0×10^{-14}	20
$IO + C_2H_5O \rightarrow$ products	4.0×10^{-11}	*b*
$I + C_2H_5O \rightarrow$ products	8.5×10^{-11}	*b*
$I + C_2H_5O_2 \rightarrow$ products	3.7×10^{-11}	*c*
$I + C_2H_5 \rightarrow C_2H_5I$	1.2×10^{-11}	44
diffusion rate	200	this work

[a] Reactions concerning I and IO listed in Table 1 were included in simulation. [b] Same values for CH_3O_2 and CH_3O were assumed. [c] Same value for the reaction of I with CF_3O_2 was assumed.

TABLE 4: Reactions Used in Kinetic Simulation for IO + CF_3O_2 at 298 K, 100 Torr Total Pressure of N_2 Diluent[a]

reaction	rate constant (cm^6 molecule^{-2} s^{-1} or cm^3 molecule^{-1} s^{-1} or s^{-1})	ref
$CF_3I + O(^3P) \rightarrow IO + CF_3$	3.7×10^{-12}	21
$\rightarrow$ others	7.5×10^{-13}	21
$IO + CF_3O_2 \rightarrow$ products	best-fit parameter	this work
$CF_3 + O_2 + M \rightarrow CF_3O_2 + M$	2.9×10^{-29}	20
$2CF_3O_2 \rightarrow 2CF_3O + O_2$	1.7×10^{-12}	42
$CF_3 + CF_3O_2 \rightarrow 2CF_3O$	4.0×10^{-12}	4
$CF_3O_2 + CF_3O \rightarrow$ products	1.0×10^{-10}	46
$CF_3O_2 + I \rightarrow$ products	3.7×10^{-11}	27
$2CF_3 \rightarrow C_2F_6$	1.0×10^{-11}	47
$CF_3 + IO \rightarrow I + CF_3O$	6.4×10^{-12}	48
$\rightarrow$ others	9.6×10^{-12}	48
$CF_3O + IO \rightarrow$ products	4.0×10^{-11}	*b*
$CF_3 + I \rightarrow CF_3I$	1.5×10^{-11}	49
diffusion rate	200	this work

[a] Reactions concerning I and IO listed in Table 1 were included in simulation. [b] Same value for CH_3O was assumed.

was derived using the reported absorption cross-section of OIO at 549.1 nm,[23] the upper limit of the branching ratio of reaction 1a was determined to be <0.1.

Reactions of IO with $C_2H_5O_2/CF_3O_2$. For IO + $C_2H_5O_2$ experiments, IO was produced from the reaction $O(^3P) + C_2H_5I$ with the IO production yield of 0.1−0.2 at 298 K.[28,29] The initial concentrations of C_2H_5, I, and O were estimated by the following equations;

$$[C_2H_5]_0 = [I]_0 = \frac{\sigma_{C_2H_5I}[C_2H_5I][O]_0}{\sigma_{O_3}[O_3]} \quad (13)$$

$$[IO]_0 = \beta[O]_0 \quad (14)$$

The factor $\beta = (0.15 \pm 0.05)$ is the reported branching ratio for IO formation from O + C_2H_5I.[28] The rate constant of $C_2H_5O_2$ + IO was also determined using the kinetic simulations with the chemical reactions listed in Table 3. The best-fit procedure results in $k_2 = (1.4 \pm 0.6) \times 10^{-10}$ cm^3 molecule^{-1} s^{-1} at 298 K, 100 Torr total pressure of N_2 diluent. The quoted uncertainty is derived considering all of the uncertainties of σ_{IO}, β,

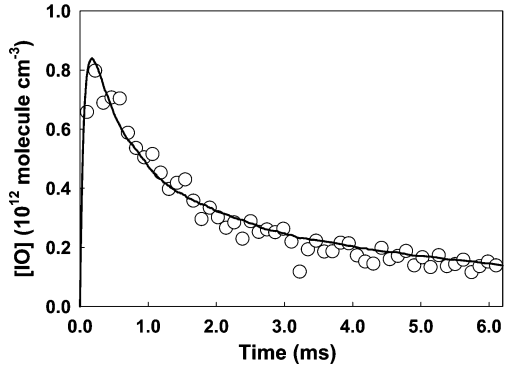

Figure 5. A typical decay time profile of IO in the presence of CF_3O_2 at 298 K and 100 Torr total pressure of N_2 diluent. $[CF_3I] = 2.5 \times 10^{15}$, $[O_3] = 1.6 \times 10^{13}$, $[CF_3]_0 = 1.1 \times 10^{13}$ molecule cm^{-3}. Thick fitting curve is the result of simulations (see text for details).

estimation of $[IO]_0$, measurements in pressure, mass flow rates, and reaction path length, and simulation fittings. The concentration of C_2H_5I was varied between $(1.0-3.2) \times 10^{15}$ molecule cm^{-3} and dissociation laser intensity was changed between 34−59 mJ $pulse^{-1}$.

For IO + CF_3O_2 experiments, IO was produced from the reaction $O(^3P)$ with CF_3I with an IO production yield of 0.83 at 298 K.[21] The concentration of O_3 was varied between $(0.7-1.6) \times 10^{13}$ molecule cm^{-3}. The dissociation laser intensity was changed between 13−41 mJ $pulse^{-1}$. By using the kinetic simulations with the chemical reactions listed in Table 4, the rate constant of IO + CF_3O_2 was determined to be $(6.3 \pm 2.7) \times 10^{-11}$ cm^3 $molecule^{-1}$ s^{-1} at 298 K, 100 Torr total pressure of N_2 diluent, as shown in Figure 5.

4. Discussion

Product Branching Ratios for IO + CH_3O_2. A weak positive temperature dependence for reaction 1 may suggest that direct abstraction of O or H atoms from CH_3O_2 may occur:

$$CH_3O_2 + IO \rightarrow CH_3O + OIO \quad \Delta H^4 = -30.7 \text{ kJ mol}^{-1} \tag{1a}$$

$$\rightarrow CH_3O + IOO \quad \Delta H^4 = -11.1 \text{ kJ mol}^{-1} \tag{1b}$$

$$\rightarrow CH_2O_2 + HOI \quad \Delta H^4 = -6.5 \text{ kJ mol}^{-1} \tag{1c}$$

The upper limit of the branching ratio of reaction 1a is determined to be <0.1 as described above. IOO radical from reaction 1b would be expected to decompose to I + O_2 at the present pressure and temperature conditions.

$$CH_3O_2 + IO \rightarrow CH_3O + I + O_2 \tag{1b'}$$

There are some reports on CH_3O formation from the analogous reaction of ClO with CH_3O_2.[30−32] The rate constant of CH_3O formation from the reaction of ClO with CH_3O_2 shows a positive temperature dependence.[30] The activation energy of the reaction of ClO with CH_3O_2 was reported to be 0.9 ± 0.3 kJ mol^{-1} by Helleis et al.,[30] which is close to the present value of the reaction of IO with CH_3O_2, 1.4 ± 0.6 kJ mol^{-1}. Therefore, the reaction path (1b) or (1b′) is most likely. Concerning reaction 1c, direct H-atom abstraction by IO with a rate constant on the order of 10^{-11} would not be likely.[33] Hence, reaction 1c would not occur. It is, however, noted that the dominant formation of HOBr in the reaction of BrO with CH_3O_2 was reported.[34]

Bale et al. suggested that one of the most likely products is CH_3OI in reaction 1.[4]

$$CH_3O_2 + IO \rightarrow CH_3OI + O_2 \quad \Delta H^{35} = -171.8 \text{ kJ mol}^{-1} \tag{1d}$$

Formation of CH_3OCl from the analogous reaction of ClO with CH_3O_2 was reported experimentally[36−38] and theoretically.[39] If reaction 1d were dominant, a negative temperature dependence of the rate constant would be expected, because this reaction could proceed via the CH_3OOOI complex.[37,39,40]

$$CH_3O_2 + IO \rightarrow [CH_3OOOI] \rightarrow CH_3OI + O_2 \tag{1d}$$

However, the present results, that is, positive temperature dependence of the rate constants, indicate that reaction 1d is not dominant. We conclude that the most likely reaction paths are 1b and/or 1b′.

Comparison of the Rate Constants. The obtained k_1 value at 298 K is in excellent agreement with that of Bale et al.,[4] $(6.0 \pm 1.3) \times 10^{-11}$ cm^3 $molecule^{-1}$ s^{-1} at 2.5 Torr He diluent.

The order of the rate constants of IO + RO_2 is $C_2H_5O_2$ > CH_3O_2 > CF_3O_2. As discussed above, the most likely reaction path in reaction 1 is formation of IOO and/or I + O_2 via the attack to O atom in CH_3O_2 by IO. A similar reaction mechanism may occur in the reaction of IO + $C_2H_5O_2$ and IO + CF_3O_2. The order of the electron density of the terminal O in RO_2 is $C_2H_5O_2$ > CH_3O_2 > CF_3O_2. Hence, the reactivity of RO_2 toward IO could be determined by the electron density. This argument could not apply to the reaction of IO + HO_2, because the dominant reaction product is HOI + O_2 with H-atom abstraction by IO.

The rate constant of the reaction of IO with CF_3O_2 determined in the present study is somewhat larger than that of Bale et al., $(3.7 \pm 0.9) \times 10^{-11}$ cm^3 $molecule^{-1}$ s^{-1}.[4] This discrepancy might be explained by the unknown pressure dependence of the reactions (e.g., IO + CF_3O), since the pressure conditions of ours and that of Bale et al. are significantly different (100 Torr of N_2 vs 2.5 Torr of He).

In our previous study of IO + CH_3SCH_3, the 266-nm photodissociation of CF_3I was used as a source of IO in the presence of O_3 and O_2.[17] We now found that the formation of CF_3O_2 from the third-body reaction of CF_3 + O_2 + M may affect the IO decay under the conditions of our previous work.

$$CF_3 + O_2 + M \rightarrow CF_3O_2 + M \tag{15}$$

$$IO + CF_3O_2 \rightarrow \text{products} \tag{3}$$

The larger the number density of M used, the more CF_3O_2, which reacts with IO, was generated.

Conclusion

The reactions of iodine monoxide radical, IO, with alkyl peroxide radicals, RO_2 (R = CH_3, C_2H_5, and CF_3), have been studied using cavity ring-down spectroscopy. The rate constant of the reaction IO + CH_3O_2 was determined to be $(7.0 \pm 3.0) \times 10^{-11}$ cm^3 $molecule^{-1}$ s^{-1} at 298 K and 100 Torr of N_2 diluent, which could apply to atmospheric modeling in the marine boundary layer. The most likely products of reaction 1 are I atom and/or IOO; hence, the reaction of IO with CH_3O_2 has the potential to affect iodine chemistry in the troposphere in a way leading to tropospheric ozone depleting.

Acknowledgment. We are grateful to Prof. S. Aloisio of California State University, Channel Islands, for helpful discussions. S.E. thanks the JSPS Research Fellowship for Young Scientists. This work is supported partly by a Grant from the COE project of Kyoto University.

References and Notes

(1) Carpenter, L. J. *Chem. Rev.* **2003**, *103*, 4953.
(2) Saiz-Lopez, A.; Plane, J. M. C. *Geophy. Res. Lett*. **2004**, *31*, L04112.
(3) Calvert, J. G.; Lindberg, S. E. *Atmos. Environ*. **2004**, *38*, 5087.
(4) Bale, C. S. E.; Canosa-Mas, C. E.; Shallcross, D. E.; Wayne, R. P. *Phys. Chem. Chem. Phys*. **2005**, *7*, 2164.
(5) O'Dowd, C. D.; Jimenez, J. L.; Bahreini, R.; Flagan, R. C.; Seinfeld, J. H.; Kulmala, M.; Pirjola, L.; Hoffmann, T. *Nature (London)* **2002**, *417*, 632.
(6) Burkholder, J. B.; Curtius, J.; Ravishankara, A. R.; Lovejoy, E. R. *Atoms. Phys. Chem*. **2004**, *4*, 19.
(7) McFiggans, G. *Nature (London)* **2005**, *433*, 7026.
(8) Pechtl, S.; Lovejoy, E. R.; Burkholder, J. B.; von Glasow, R. *Atoms. Phys. Chem. Discuss*. **2005**, *5*, 9907.
(9) Saiz-Lopez, A.; Plane, J. M. C.; McFiggans, G.; Williams, P. I.; Ball, S. M.; Bitter, M.; Hongwei, C.; Hoffmann, T. *Atoms. Phys. Chem. Discuss*. **2005**, *5*, 5405.
(10) von Glasow, R.; Sander, R.; Bott, A.; Crutzen, P. J. *J. Geophys. Res.* **2002**, *107*, 4341.
(11) McFiggans, G.; Allan, B.; Coe, H.; Plane, J. M. C.; Carpenter, L. J.; O'Dowd, C. *J. Geophys. Res.* **2000**, *105*, 371.
(12) Stutz, J.; Hebestreit, K.; Alicke, B.; Platt, U. *J. Atmos. Chem*. **1999**, *34*, 65.
(13) Burkert, J.; Andres-Hernandez, M. D.; Stobener, D.; Burrows, J. P.; Weissenmayer, M.; Kraus, A. *J. Geophys. Res.* **2001**, *106*, 5457.
(14) O'Keefe, A.; Deacon, D. A. G. *Rev. Sci. Instrum*. **1988**, *59*, 2544.
(15) Wheeler, M. D.; Newman, S. M.; Orr-Ewing, A. J.; Ashfold, M. N. R. *J. Chem. Soc., Faraday. Trans.* **1998**, *94*, 337.
(16) Yu, T.; Lin, M. C. *J. Am. Chem. Soc.* **1993**, *115*, 4371.
(17) Nakano, Y.; Enami, S.; Nakamichi, S.; Aloisio, S.; Hashimoto, S.; Kawasaki, M. *J. Phys. Chem. A* **2003**, *107*, 6381.
(18) Enami, S.; Hoshino, Y.; Ito, Y.; Hashimoto, S.; Kawasaki, M.; Wallington, T. J. *J. Phys. Chem. A* **2006**, *110*, 3546.
(19) Brown, S. S.; Ravishankara, A. R.; Stark, H. *J. Phys. Chem. A* **2000**, *104*, 7044.
(20) Sander, S. P.; Friedl, R. R.; Ravishankara, A. R.; Golden, D. M.; Kolb, C. E.; Kurylo, M. J.; Huie, R. E.; Orkin, V. L.; Molina, M. J.; Moortgat, G. K.; Finlayson-Pitts, B. J. *Chemical Kinetics and Photochemical Data for Use in Stratospheric Modeling: Evaluation 14*; Jet Propulsion Laboratory: Pasadena, California, 2003.
(21) Gilles, M. K.; Turnipseed, A. A.; Talukdar, R. K.; Rudich, Y.; Peter, W. V.; Huey, L. G.; Burkholder, J. B.; Ravishankara, A. R. *J. Phys. Chem.* **1996,** *100*, 14005.
(22) Enami, S.; Ueda, J.; Goto, M.; Nakano, Y.; Aloisio, S.; Hashimoto, S.; Kawasaki, M. *J. Phys. Chem. A* **2004,** *108*, 6347.
(23) Spietz, P.; Martin, J. C. G.; Burrows, J. P. *J. Photochem. Photobiol., A* **2005**, *176*, 50.
(24) Newman, S. M.; Howie, W. H.; Lane, I. C.; Upson, M. R.; Orr-Ewing, A. J. *J. Chem. Soc., Faraday. Trans.* **1998,** *94*, 2681.
(25) Harwood, M. H.; Burkholder, J. B.; Hunter, M.; Fox, R. W.; Ravishankara, A. R. *J. Phys. Chem.* **1997,** *101*, 853.
(26) Bloss, W. J.; Rowley, D. M.; Cox, R. A.; Jones, R. L. *J. Phys. Chem.* **2001,** *105*, 7840.
(27) Canosa-Mas, C. E.; Vipond, A.; Wayne, R. P. *Phys. Chem. Chem. Phys*. **1999**, *1*, 761.
(28) Monks, P. S.; Stief, L. J.; Tardy, D. C.; Liebman, J. F.; Zhang, Z.; Kuo, S. C.; Klemm, R. B. *J. Phys. Chem.* **1995**, *99*, 16566.
(29) Teruel, M. A.; Dillon, T. J.; Horowitz, A.; Crowley, J. N. *Phys. Chem. Chem. Phys.* **2004**, *6*, 2172.
(30) Helleis, F.; Crowley, J. N.; Moortgat, G. K. *J. Phys. Chem.* **1993**, *97*, 11464.
(31) Biggs, P.; Canosa-Mas, C. E.; Fracheboud, J. M.; Shallcross, D. E.; Wayne, R. P. *Geophys. Res. Lett*. **1995**, *22*, 1221.
(32) Kukui, A. S.; Jungkamp, T. P. W.; Schindler, R. N. *Ber. Bunsen-Ges. Phys. Chem.* **1994**, *98*, 1298.
(33) Buben, S. N.; Larin, I. K.; Trofimova, E. M. *Kinet. Katal.* **1995**, *36*, 74.
(34) Aranda, A.; Le Bras, G.; Laverdet, G.; Poulet, G. *Geophys. Res. Lett.* **1997**, *24*, 2745.
(35) Misra, A.; Berry, R. J.; Marshall, P. *J. Phys. Chem. A* **1997**, *101*, 7420.
(36) Kenner, R. D.; Ryan, K. R.; Plumb, I. C. *Geophys. Res. Lett.* **1993**, *20*, 1571.
(37) Helleis, F.; Crowley, J.; Moortgat, G. *Geophys. Res. Lett*. **1994**, *21*, 1795.
(38) Daele, V.; Poulet, G. J. *Chim. Phys. Physico-Chim. Biol*. **1996,** *93*, 1081.
(39) Drougas, E.; Jalbout, A. F.; Kosmas, A. M. *J. Phys. Chem. A* **2003**, *107*, 11386.
(40) Guha, S.; Francisco, J. S. *J. Chem. Phys.* **2003**, *118*, 1779.
(41) Canosa-Mas, C. E.; Flugge, M. L.; Shah, D.; Vipond, A.; Wayne, R. P. *J. Atmos. Chem.* **1999**, *34*, 153.
(42) Atkinson, R.; Baulch, D. L.; Cox, R. A.; Crowley, J. N.; Hampson, R. F., Jr.; Kerr, J. A.; Rossi, M. J.; Troe, J. *IUPAC Subcommittee on Gas Kinetic Data Evaluation for Atmospheric Chemistry*; 2004.
(43) Shah, D.; Canosa-Mas, C. E.; Hendy, N. J.; Scott, M. J.; Vipond, A, Wayne, R. P. *Phys. Chem. Chem. Phys.* **2001**, *3*, 4932.
(44) Hunter, T. F.; Kristjansson, K. S. *J. Chem. Soc., Faraday Trans. 2* **1982**, *78*, 2067.
(45) Jenkin, M. E.; Cox, R. A.; Mellouki, A.; Le Bras, G.; Poulet, G. *J. Phys. Chem.* **1990**, *94*, 2927.
(46) Nielsen, O. J.; Sehested, J. *Chem. Phys. Lett.* **1993**, *213*, 433.
(47) Pagsberg, P.; Jodkowski, J. T.; Ratajczak, E.; Sillesen, A. *Chem. Phys. Lett.* **1998**, *286*, 138.
(48) Vipond, A.; Canosa-Mas, C. E.; Flugge, M. L.; Gray, D. J.; Shallcross, D. E.; Shah, D.; Wayne, R. P. *Phys. Chem. Chem. Phys.* **2002**, *4*, 3648.
(49) Skorobogatov, G. A.; Slesar, O. N.; Torbin, N. D. *Vestn. Leningr. Univ., Ser. 4: Fiz. Khim.* **1988**, *1*, 30.